Fission – a complete laboratory

Karl-Heinz Schmidt
D-64390 Erzhausen, Germany

ABSTRACT

A review on the progress in experimental methods, experimental results and theoretical ideas of the last decades in the field of nuclear fission is given. New approaches extended the availability of fissioning systems for experimental studies on low-energy fission considerably and provided a full identification of all fission products in A and Z for the first time. The systematics of available data gives a more comprehensive view on the influence of shell effects and pairing correlations on the fission-fragment mass and nuclear-charge distributions. These data reveal that in asymmetric fission of the actinides the position of the heavy component in Z is approximately constant. Theoretical arguments for this unexpected finding are not yet available. The modelling of the fission process with dynamical models is still very difficult, since most advanced models in nuclear physics that have been developed for stationary states are not readily applicable to the decay of a meta-stable state. Semi- empirical methods exploiting powerful theoretical ideas like (i) the separability of the influences of fragment shells and macroscopic influences of the compound nucleus, (ii) the properties of a quantum oscillator coupled to the heat bath of the other nuclear degrees of freedom for describing the fluctuations of normal collective modes, and (iii) an early freeze-out of collective motion to include dynamical effects seem to give a good description of the observed general trends and reach a precision needed for technical applications. The transformation of part of the fission Q value into intrinsic excitation energy along the fission process and the division between the fragments, following the laws of statistical mechanics, is essential for explaining the observed features of prompt-neutron emission and the even-odd effect in fission-fragment element yields. The importance of nuclear fission as a laboratory for studying the dynamics of non-equilibrium processes in mesoscopic objects under the influence of residual interactions is stressed.

Preprint of a contribution to the proceedings of the Joliot-Curie school, Nice, France, 12th - 17th Sept. 2011.

Contents

I. INTRODUCTION

Since the discovery of nuclear fission by Hahn and Straßmann in 1939 [1], the progress in the understanding of this dramatic nuclear re-organization process has not ceased being stimulated by new experimental findings. Although the gross explanation of nuclear fission on the basis of the liquid- drop model was provided very soon by Bohr and Wheeler [2], new observations permanently revealed a more and more detailed view on the complexity of nuclear fission and created new challenges for theory. Research on nuclear fission, in particular low-energy fission, where the influence of nuclear structure is strong, also yielded profit for the understanding of nuclear properties in general. The observation of asymmetric fission promoted the development of the nuclear shell model [3, 4]. The existence of shape isomers proved that shell effects persist at large deformations [5]. In the 1980's, a rather comprehensive understanding of the fission process had seemed to be reached, which is documented in the well-known text book of Wagemans [6]. Among the most important achievements were the development of the concept of fission channels [7] and the study of the even-odd effect in fission-fragment Z distributions [8, 9]. But new discoveries in the domain of nuclear fission are emerging continuously up to present times. The present contribution emphasizes some new theoretical ideas, which solve long-standing problems, and a few very recent findings, which represent new puzzles to theory.

II. GENERAL REMARKS

The discovery of fission revealed that the ground state of the heaviest nuclei is barely bound. An excitation energy in the order of a few percent of their total binding energy is sufficient to induce the disintegration into two pieces in a collective shape evolution that resembles the division of living cells, releasing a huge amount of energy of about 200 MeV, see figure 1. Thus, the energy content of nuclear fuel is about 10^8 times larger compared to fossil fuels like coal, mineral oil or natural gas, which explains the importance of nuclear technology. Figure 2 shows the binding energy per nucleon according to the liquid-drop model as a function of the nuclear mass. The binding energy per nucleon decreases for light nuclei due to the increasing surface energy, and it decreases for heavy nuclei due to the increasing Coulomb energy. Thus, energy is released in the fusion of light nuclei and in the fission of heavy nuclei. The energy stored in heavy nuclei, and even the synthesis of an appreciable portion of matter in the Universe has its origin in the r-process, a process of consecutive neutron capture and beta decay in an environment with a very high neutron flux in some astrophysical site, which is not yet fully identified [10].

Nuclear fission offers a rich laboratory for a broad variety of scientific research on nuclear properties, astrophysics and general physics. The r-process nucleosynthesis cannot be fully understood without a precise knowledge of the fission properties of very neutron-rich isotopes of the heaviest elements, which are presently not accessible to direct measurements [11]. The relatively flat potential energy reaching to very large deformations allows studying nuclear properties like shell effects in super- and hyper-deformed shapes [12]. Phenomena connected with the decay of the quasi-bound nuclear

system beyond the fission barrier yield information on nuclear transport properties like nuclear viscosity [13] and heat transfer between the nascent fragments [14]. They even offer a valuable test ground of general importance for non-equilibrium processes in mesoscopic systems, where quantum mechanics and microcanonical thermodynamics play an important role [15].

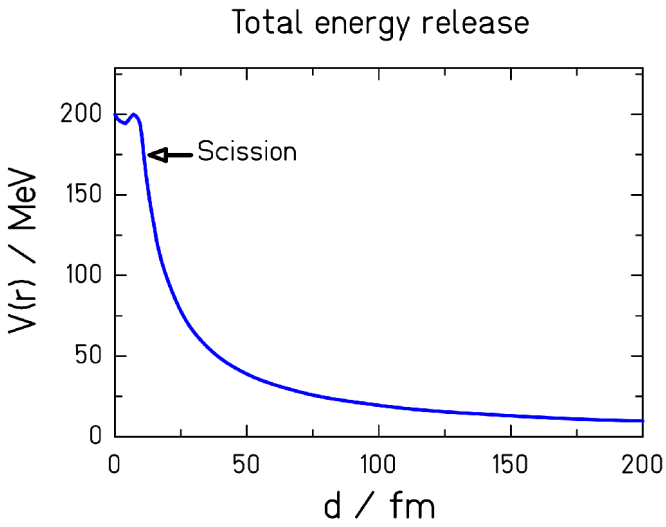

Figure 1. *Potential energy released in the fission of ^{238}U as a function of the distance d between the centres of the fragments. Shell effects are neglected. In the mono-nuclear regime, d denotes the distance between the centres-of-mass of the two halves of the nucleus [16].*

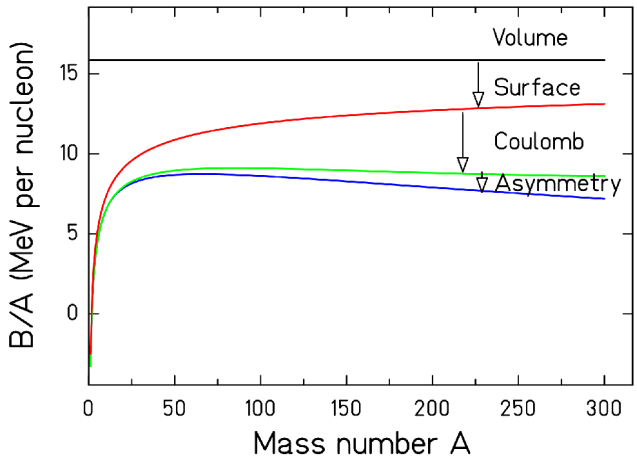

Figure 2. *The different contributions to the binding energy per nucleon of nuclei along the beta-stability line according to the liquid-drop model [17]. The total binding energy per nucleon (blue line) is maximum around A = 56. Lighter nuclei as well as heavier nuclei are less bound.*

Even after more than 70 years of intense research, nuclear fission is still far from being fully understood. The present status in experimental knowledge and theoretical understanding is not yet satisfactory. There exist a number of valuable experimental signatures of fission like the mass and nuclear-charge division, the fragment kinetic energies as well as prompt neutron and gamma yields. However, overcoming present restrictions in the choice of fissioning systems and obtaining the necessary experimental resolution still requires substantial technological effort. The theoretical understanding of the fission process cannot fully rely on the powerful standard methods conceived for describing static nuclear properties; it requires developing new methods for modelling non-equilibrium processes in nuclei, e.g. [18, 19]. At present, combining available experimental information, e.g. [20, 21] with a large variety of long-standing and newly developed theoretical ideas proves to be the most successful approach for quantitative predictions to be used in nuclear technology and for considerable progress in understanding certain aspects of nuclear fission [22, 23].

III. EXPERIMENTAL METHODS

Available fissionable nuclei

The progress in the understanding of fission heavily relied and still relies on the development of advanced experimental methods. A severe restriction is still the availability of fissionable material as target material. Therefore, the traditional use of neutrons for inducing fission offers only a rather limited choice of fissioning systems. These limitations were more and more overcome by alternative methods: Spontaneously fissioning heavy nuclei were produced by fusion reactions [24]. Exotic nuclei were produced in spallation reactions which undergo beta-delayed fission [25]. Electromagnetic-induced fission of neutron-deficient radioactive nuclei, produced as projectile fragments from a ^{238}U primary beam, was studied in-flight at relativistic energies [26]. Very recently, comprehensive studies on fission of transfer products of ^{238}U projectiles have been performed [27]. Very interesting experiments on fission of fragments of ^{238}U relativistic projectiles by tagged photons will be possible with the ELISE electron-ion collider ring at the future FAIR facility [28].

Detection and resolution

The identification of fission products poses a severe problem. First experiments, which were based on radiochemical methods [29], were not fast enough to determine the yields of short-lived fragments and suffered from normalization problems. Kinematic identification methods by double time-of-flight [30, 31] and double-energy measurements [32] provided full mass distributions, however with limited resolution. The LOHENGRIN spectrograph brought big progress in identifying the masses and the nuclear charges of the light fission products [33]. However, full isotopic identification (in Z and A) of all fission products has only been achieved by boosting the energies of the products in inverse-kinematics experiments and using powerful magnetic spectrometers [26, 27, 34].

IV. FISSION CHANNELS

Symmetric and asymmetric fission

Bohr and Wheeler [2] explained the phenomenon of nuclear fission by the influence of the Coulomb repulsion in heavy nuclei that favours elongated shapes and, finally, the separation onto two fragments of preferentially equal size. Figure 3 schematically shows the height of the barrier, which stabilizes the nucleus against fission, as a function of mass asymmetry. In light nuclei, the surface energy dominates, and the barrier for symmetric splits is maximum. In heavy nuclei, the Coulomb energy is decisive, and the barrier for symmetric splits is minimum. The fission-barrier height in ^{235}U is only about 5 MeV.

However, Bohr and Wheeler could not explain the predominant asymmetric mass division in the fission of the actinides. Maria Goeppert-Maier [3] traced the asymmetric fission back to nuclear shell effects, in particular to the stabilizing influence of the 50 proton shell and the 82 neutron shell that coincide in the spherical doubly magic ^{132}Sn. The existence of shell effects in deformed nuclei, which play an even more important role in nuclear fission, evidenced by the existence of shape isomers [35] and shell-stabilized strongly deformed fragments at scission [36], was introduced later by S. G. Nilsson [5].

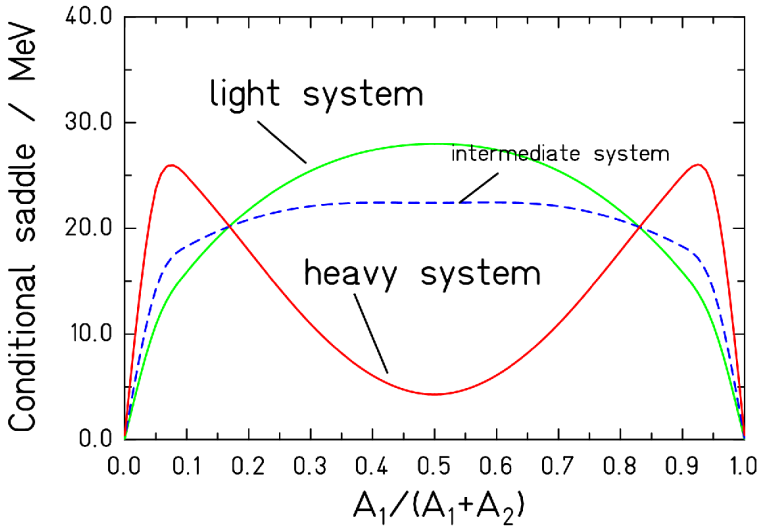

Figure 3. *Schematic presentation of the fission-saddle height under the condition of a specific mass asymmetry according to the liquid-drop model.*

Experimental systematics

Figure 4 gives an overview on the measured mass and nuclear-charge distributions of fission products from low-energy fission. Fission of target nuclei in the actinide region, mostly induced by neutrons, shows predominantly asymmetric mass splits. A transition to symmetric mass splits is seen around mass 258 in spontaneous fission of fusion residues. Electromagnetic-induced fission of relativistic secondary beams covers the transition from asymmetric to symmetric fission around mass 226. A pronounced fine structure

close to symmetry appears in ^{201}Tl [37] and in ^{180}Hg [25]. It is difficult to observe low-energy fission in this mass range. Thus, ^{201}Tl could only be measured down to 7.3 MeV above the fission barrier due to its low fissility, which explains the filling of the minimum between the two peaks. Only ^{180}Hg was measured at energies close to the barrier after beta decay of ^{180}Tl. Considering the measured energy dependence of the structure for ^{201}Tl [25], the fission characteristics of these two nuclei are rather similar. Also other nuclei in this mass region show similar features [38].

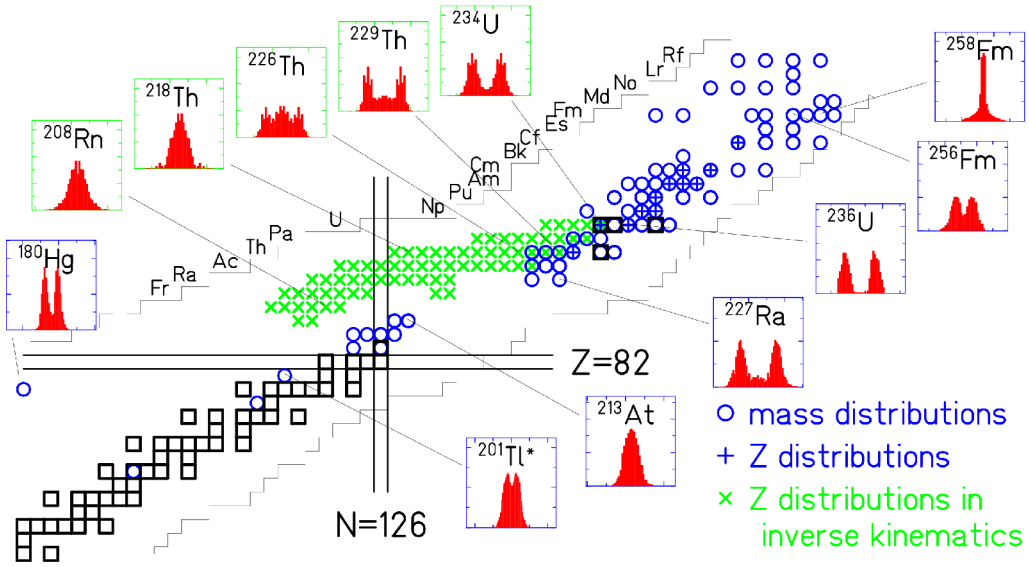

Figure 4. *General view on the systems for which mass or nuclear-charge distributions have been measured. The distributions are shown for 12 selected systems. Blue circles (blue crosses): Mass (nuclear-charge) distributions, measured in conventional experiments [25, 37] and references given in [26]. Green crosses: Nuclear-charge distributions, measured in inverse kinematics [26].*

Size of the heavy fragment in asymmetric fission

In the range where asymmetric fission prevails, e.g. from ^{227}Ra to ^{256}Fm, the light and the heavy fission-product components gradually approach each other with increasing mass of the fissioning nucleus, see figure 4. A quantitative analysis reveals that the mean mass of the heavy component stays approximately constant [39] at about A=140. This has been explained by the influence of a deformed (β≈0.6) fragment shell at N=88 and the spherical shell at N=82 [36], suggesting that the position of the heavy fragment is essentially constant in neutron number.

New data on Z distributions over long isotopic chains [26], however, reveal very clearly that the position in neutron number varies systematically over more than 7 units, while the position in proton number is approximately constant at Z=54, see figure 5. The rather short isotopic sequences covered in former experiments did not allow deducing this feature and gave the false impression of a constant position in mass.

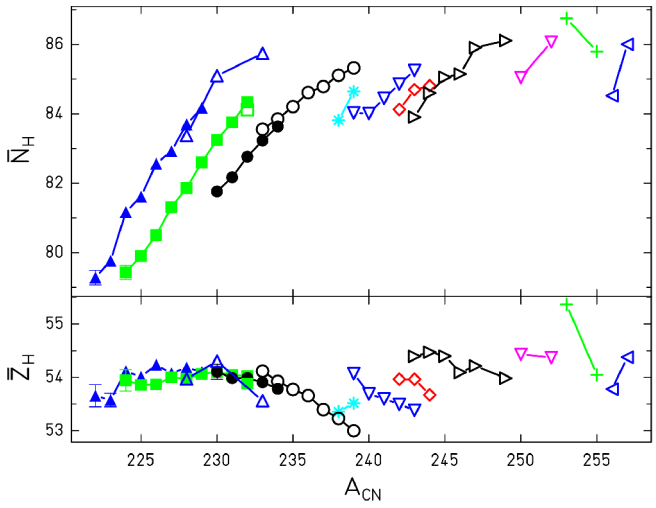

Figure 5. *Mean neutron and proton number of the heavy component in asymmetric fission in the actinide region. The values were deduced from measured mass and nuclear-charge distributions using the semi-empirical GEF code [*[23]*] for the correction of charge polarization and prompt-neutron emission. Open symbols denote results from conventional experiments, full symbols refer to an experiment with relativistic projectile fragments of* ^{238}*U [*[22]*]. (See [*[23]*] for references of the underlying experimental data.)*

This finding represents a severe puzzle to theory, since shell-model calculations do not show any shell stabilization near Z=54 at $\beta\approx$0.6 [[36], [40]].

Separability principle

The microscopic-macroscopic approach has proven to be very useful for calculating nuclear properties, in particular in applications to fission [[41]]. The early influence of fragment shells on the fission path, deduced from two-centre shell-model calculations [[42]], makes its application to fission even more powerful. It means that the microscopic properties of the fission observables are essentially determined by the shells of the fragments, and only the macroscopic properties are specific to the fissioning system [[43]]. This "separability principle" was exploited in the GEF code [[23]], which relies on an empirical description of the macroscopic stiffness parameters in the relevant normal modes and empirically deduced fragment shells, which are valid for all fissioning systems.

The basic ideas of the GEF code follow closely the approach introduced by Jensen and Døssing [[44]] for a statistical calculation of the mass distribution in fission, however, with a few important modifications: (i) The shell effects that were calculated from single-particle energy spectra in a Woods-Saxon potential with the Strutinsky method in ref. [[44]] are replaced by global fragment shells, which are adjusted to the measured mass distributions. The separability principle simplifies this task considerably, since the fragment shells are assumed to depend only on the fragment, and, thus, they are the same for all fissioning systems. (ii) The nuclear level density that was calculated from the same

single-particle spectrum including pairing correlations using the BCS approximation in ref. [44] is replaced by an empirical constant-temperature formula [45], which seems to be in better agreement with recent experimental results [46]. In addition, the shapes of the fragments at scission, the charge polarization, the angular momenta, and other properties of the fragments as well as the emission of prompt neutrons and gamma-rays are calculated on the basis of similar ideas. See ref. [23] for a detailed description of the code. In figures 6, 7 and 8, a comprehensive comparison of mass and nuclear-charge distributions with the results of the GEF code is shown. The data over a large range of systems can be described very well with the same parameter set. The most important values are the positions, the depths and the widths of 3 fragment shells for the standard 1, the standard 2 and the super-asymmetric fission channel, which are described with the same 14 parameter values for all systems. The narrow symmetric fission in the heaviest nuclei results from the superposition of the standard-1 shells in the two fragments and, thus, does not require any additional parameter.

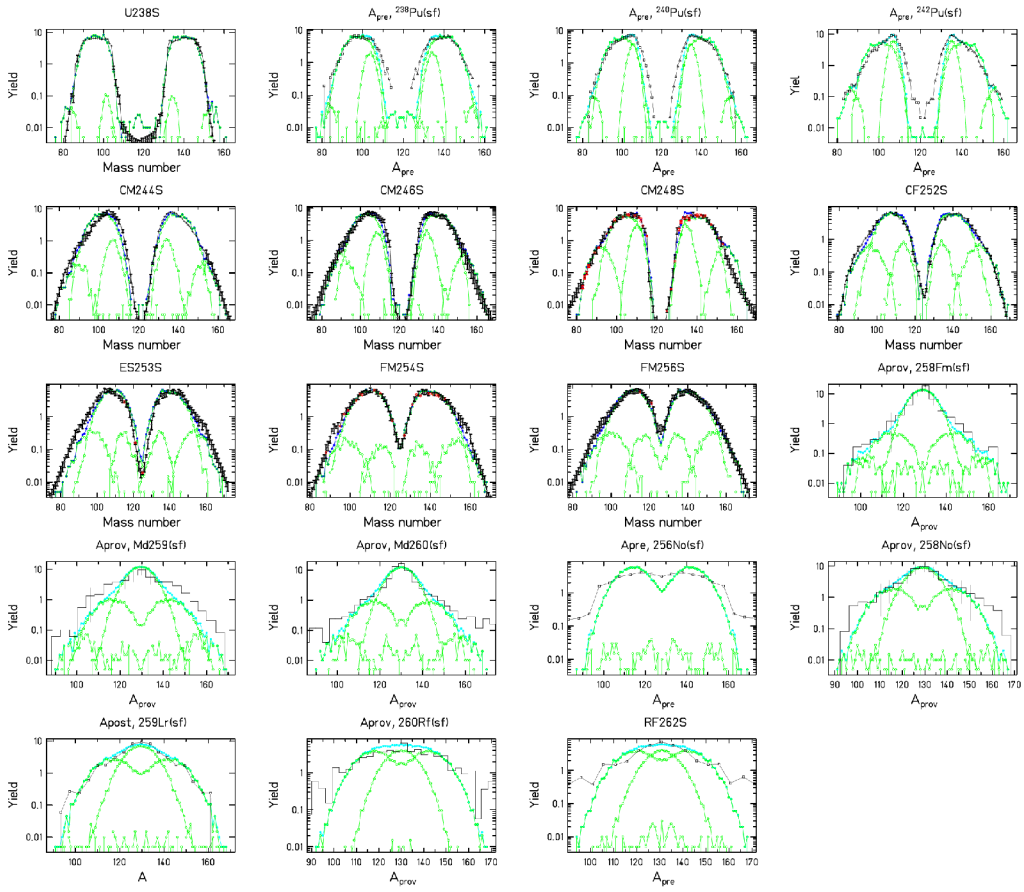

Figure 6. *Mass distributions of fission fragments from spontaneous fission. (In most cases the post-neutron values are shown. A_{prov} is the "provisional mass" that is directly deduced from the ratio of the kinetic energies of the fragments and thus not corrected for neutron emission.) Measured or evaluated data (black lines, respectively histogram) are compared with predictions of the GEF code [23] (green lines). The contributions of different fission channels are shown. (See [23] for references of the data.)*

Apparently, the complex variation of the mass distributions of the different fissioning systems has a rather simple origin on the level of the fission valleys formed by the shell effects, superimposed on the macroscopic global potential-energy surface. Some of the discrepancies are probably caused by shortcomings of the evaluated files due to insufficient experimental information, e.g. for ^{229}Th(n_{th},f) and ^{255}Fm(n_{th},f).

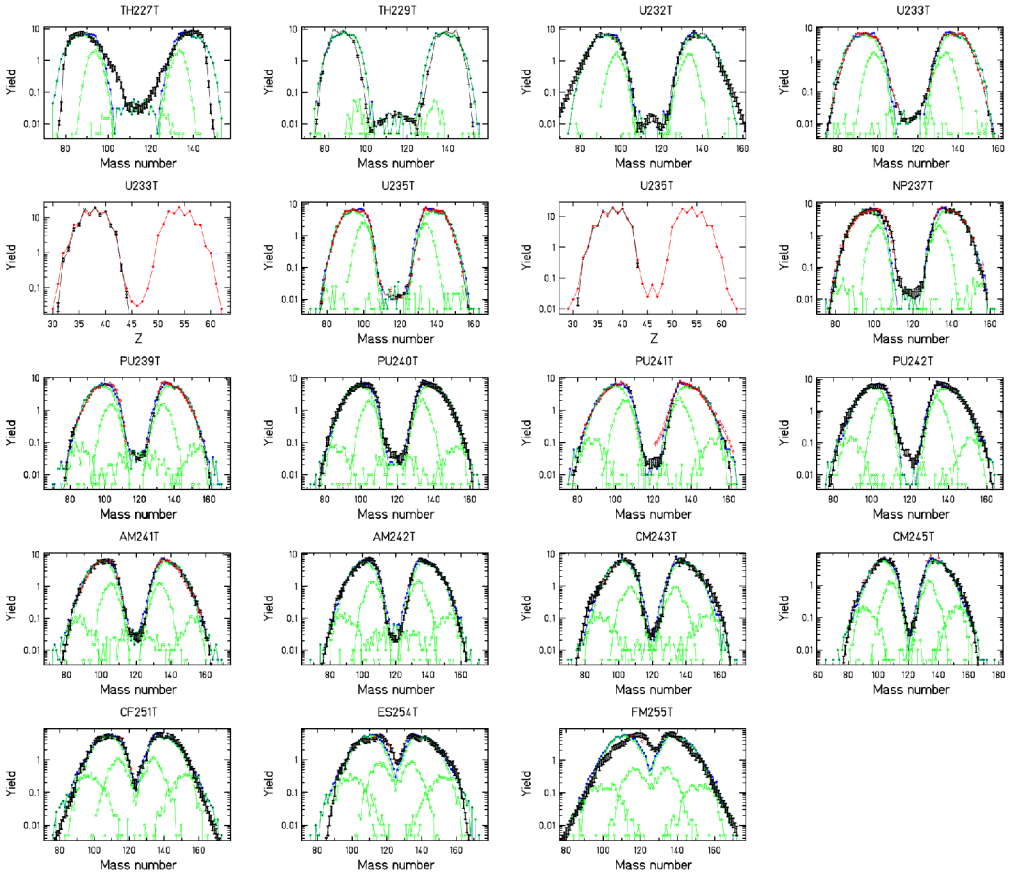

Figure 7. *Nuclear-charge and mass distributions of fission fragments from thermal-neutron-induced fission. Measured or evaluated data (black lines, respectively histogram) are compared with predictions of the GEF code [23] (red and green lines). The contributions of different fission channels are shown. (See [23] for references of the data.)*

Dynamical effects

Statistical scission-point models, e.g. ref. [36], suffer from the neglect of dynamical effects. Stochastic calculations revealed that, depending on the nature of the collective degree of freedom, dynamical effects induce a kind of memory on the fission trajectory, which may be accounted for by assuming an early freeze-out that depends on the influence of inertia. Mass-asymmetric distortions have a large inertia, and thus the mass distribution is already essentially determined slightly behind the outer fission saddle [47]. This is accounted for in the GEF code by choosing an underlying macroscopic potential

that is deduced from measured mass distributions [48]. Thus, it effectively includes dynamical effects. Charge polarization has a small inertia, and the distribution is determined close to scission [49].

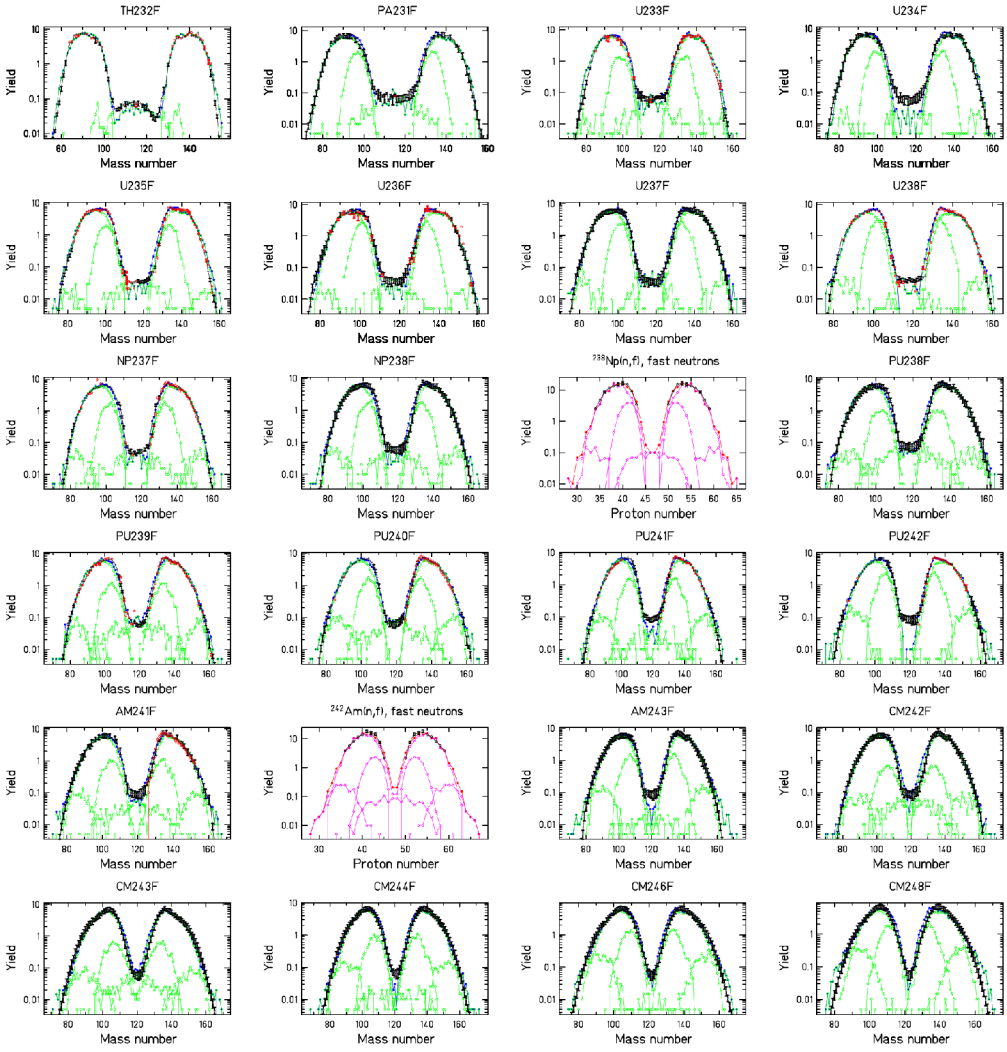

Figure 8. *Nuclear-charge and mass distributions of fission fragments from fast-neutron-induced fission. Measured or evaluated data (black lines, respectively histogram) are compared with predictions of the GEF code [23] (red and green lines). The contributions of different fission channels are shown. (See [23] for references of the data.)*

Fluctuations

Most fission observables form bell-shaped distributions around a mean value. This suggests treating the corresponding collective degree of freedom as an harmonic quantum oscillator coupled to a heat bath of temperature T with limited excitation energy. Especially for the charge-polarization degree of freedom there exists a long discussion about the importance of the zero-point motion [50, 51]. Nix estimated the level spacing in the oscillator corresponding to mass-asymmetric distortions at saddle with the liquid-drop

model to 1-2 MeV in the actinide region [52]. According to the smaller widths of the corresponding components to the mass distribution, the level spacing for oscillations in the two asymmetric fission valleys (Standard 2 and Standard 1) is about 5 and more than 10 MeV, respectively. Also for oscillations in the charge-polarization degree of freedom, the level spacing is in the order of 10 MeV. These values are appreciably larger than the temperature values of actinides, which are about 0.5 MeV in the constant-temperature regime [45]. Thus, in a statistical approach these degrees of freedom are essentially not excited, and the widths of the corresponding distributions are essentially determined by the zero-point motion.

Also the angular-momentum distributions of the fragments have been explained by "orientation pumping" due to the uncertainty principle [53]. Experimental indications for thermal excitations of spherical fragments [54] have also been explained by the compensation of the orbital angular momentum, which itself is induced by the zero-point motion [55]. Here it is the operator of the orbital angular momentum which does not commute with the angle that characterizes the direction of particle motion. Thus, all fragment angular momenta measured in low-energy fission are explained by the quantum-mechanical uncertainty principle. There is no room for excitations of the angular-momentum-bearing modes [56].

Due to the strong influence of quantum-mechanical effects it is mandatory to explicitly consider these, as it is e.g. done in the self-consistent microscopic approach of ref. [57]. Stochastic approaches with classical models, e.g. ref. [58] seem to be inadequate. In the GEF code, the influence of the zero-point motion on the different observables is considered by calculating the position distribution in the quantum oscillator [59] corresponding to the respective normal mode [52] as a function of nuclear temperature and excitation energy.

V. PROMPT-NEUTRON YIELDS

Transformation of energy – the different contributions

In low-energy fission, the available energy, consisting of the Q value of the reaction plus the initial excitation energy of the fissioning nucleus, ends up either in the total kinetic energy (TKE) or the total excitation energy (TXE) of the fragments. The TKE is closely related to the distance of the centres of the two nascent fragments at scission, but it cannot give information on the shapes of the individual fragments. The TXE, however, can be attributed to the individual fragments by a kinematical measurement of the prompt neutrons. Still, there is no direct experimental information on the processes, which are responsible for the transformation of part of the available energy into the excitation energies of the separated fragments. The situation is schematically illustrated in figure 9. Before scission, dissipation leads to intrinsic excitations, collective modes perpendicular to the fission direction (normal modes [52]) may be excited, and, finally, some energy is stored in deformation of the nascent fragments that is induced by the Coulomb repulsion. The remaining part is found as pre-scission kinetic energy [60]. After scission, collective excitations and deformation energy are transformed and add up to the intrinsic excitations of the separated fragments.

The situation at scission is important for the understanding of fission dynamics, e.g. the magnitude of dissipation and the coupling between the different collective degrees of freedom, but without additional information, the energy repartition remains ambiguous.

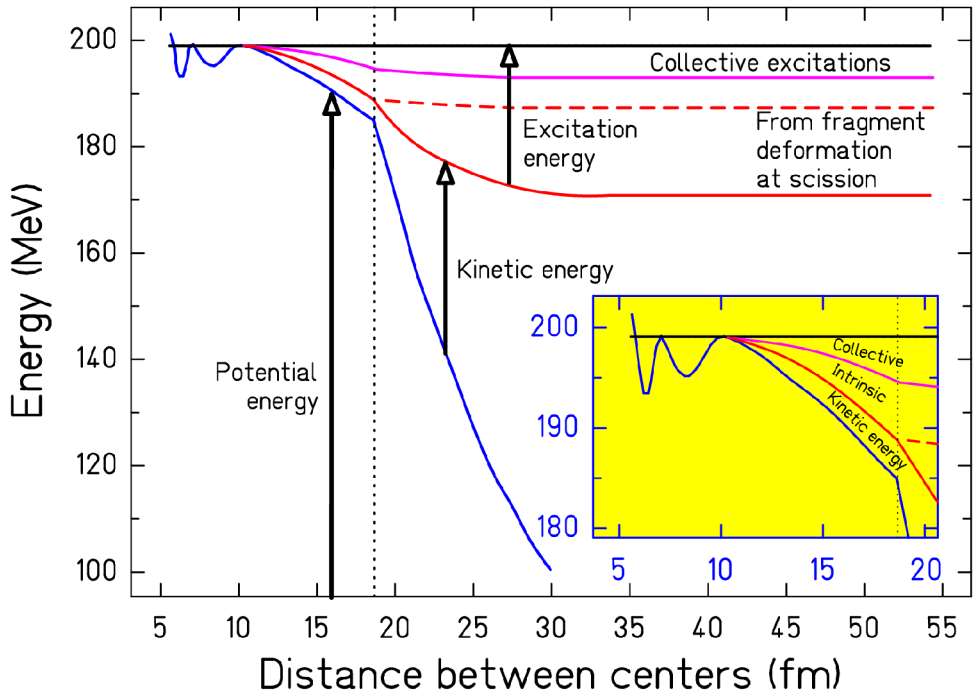

Figure 9. *Schematic drawing of the transformation of energy during the fission process of ^{236}U with an initial excitation energy equal to the height of the fission barrier. (Adapted from figs. 7 to 9 of ref. [61].)*

Origin of the saw-tooth shape

There is widespread agreement that the saw-tooth shape of the prompt-neutron yields, see figure 10, is caused by the deformation energies of the nascent fragments at scission. The scission-point model of ref. [36] attributes it to the influence of fragment shells, the random-neck-rupture model [7] links it to the location of the rupture, and also microscopic calculations predict large deformation energies of the fragments near scission [62]. Large even-odd effects in the fragment Z distributions indicate that the probability for populating the fragments in their ground state is rather high, see the dedicated discussion below. Thus, the intrinsic excitation energy at scission is generally much too low to account for the variation of the prompt-neutron yield by several units over the different fragments.

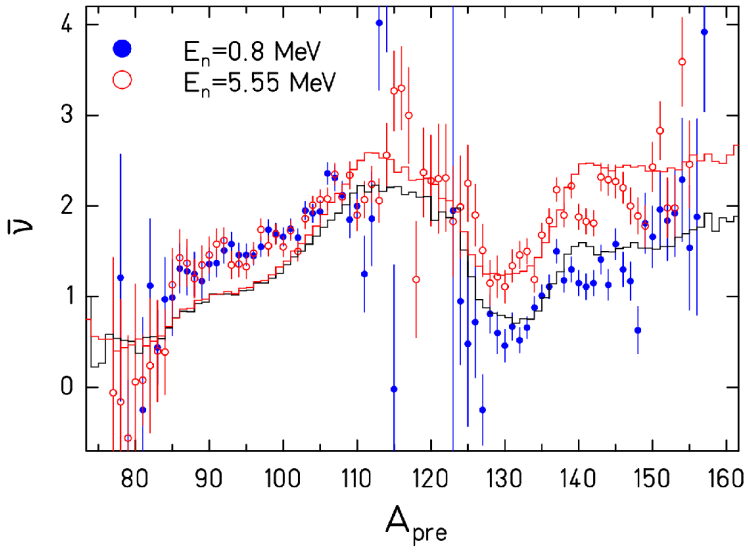

Figure 10. *Measured prompt-neutron yield in ^{237}Np(n,f) as a function of pre-neutron mass at two different incident-neutron energies [63] (data points) in comparison with the result of the GEF code [23] (histograms).*

Differential behaviour – energy sorting

Recent experimental results indicate that nuclei exhibit an essentially constant temperature T up to excitation energies of 20 MeV [46]. According to empirical systematics, the temperature parameter T is grossly proportional to $A^{-2/3}$ [45]. The temperature is deduced from the energy-dependent nuclear state density $\omega(E)$, or approximately from the energy-dependent nuclear level density $\rho(E)$ [64], defined as $T=(\mathrm{d}\ln\omega/\mathrm{d}E)^{(-1)}\approx(\mathrm{d}\ln\rho/\mathrm{d}E)^{-1}$. The constant-temperature behaviour is explained by the breaking of pairs in the so-called superfluid regime [65]. This leads to a considerable increase of the heat capacity $C=\mathrm{d}E/\mathrm{d}T$ [66] and consequently to a slow variation of temperature T as a function of excitation energy E. Note that the BCS approximation severely underestimates the pairing condensation energy E_{cond} and consequently also the magnitude of the heat capacity in the so-called superfluid regime [67]. Thus, the assumption of a constant nuclear temperature T becomes a good approximation.

The configuration before scission consists of two nuclei being in thermal contact by the neck. The two nuclei may be considered as two heat baths with different energy-independent temperatures, T_1 and T_2, and a total constant amount of excitation energy $E=E_1+E_2$. A rough estimation of the thermodynamical properties of this system may be deduced from the entropy as a function of energy division:

$$S=S_1+S_2=\frac{E_1}{T_1}+\frac{E_2}{T_2}=\frac{E_1}{T_1}+\frac{E-E_1}{T_2}=\frac{T_1E+(T_2-T_1)\cdot E_1}{T_1\cdot T_2} \qquad (1)$$

Figure 11 shows a numerical example. Since there exists no equilibrium solution with $T_1 = T_2$, one can only argue that the system develops in the direction of increasing entropy. This implies that the intrinsic excitation energy of the two nascent fragments at scission is subject to energy sorting [14, 68, 69]: The hotter light fragment transfers essentially all its intrinsic excitation energy to the colder heavy fragment.

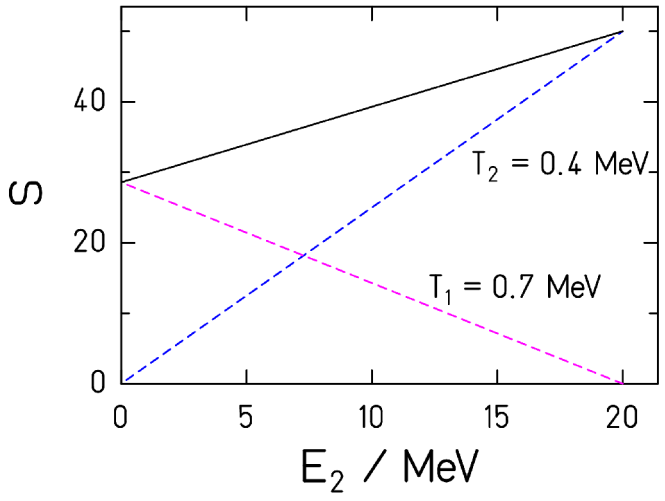

Figure 11. *Entropy of the pre-scission configuration as a function of energy division. The temperatures of the two nascent fragments are assumed to be 0.4 MeV and 0.7 MeV.*

A more realistic estimation of the energy division, based on a microscopic scenario, is illustrated in figure 12. The exchange of excitation energy between the nascent fragments may be performed by the transfer of nucleons across the neck. The different single-particle occupation functions, corresponding to the different temperatures, cause an enhanced transfer of particles from the heavy to the light fragment below the Fermi surface and an enhanced transfer of particles from the light to the heavy fragment above the Fermi surface. Both processes lead to a transport of excitation energy from the light to the heavy fragment.

This energy transport may be considered as a kind of second-order window formula. While the window formula of the one-body dissipation [70] leads to energy dissipation, that means heating of both reaction partners, due to the relative velocity of the reaction partners, the energy sorting in fission is caused by the different slopes of the single-particle occupation functions. Fission provides a rather unique scenario for the phenomenon of energy sorting between nuclei, because the relative velocity of the nascent fragments before fission is very small compared to the Fermi velocity, and thus the heating due to one-body dissipation is small. This is not the case in most nuclear reactions.

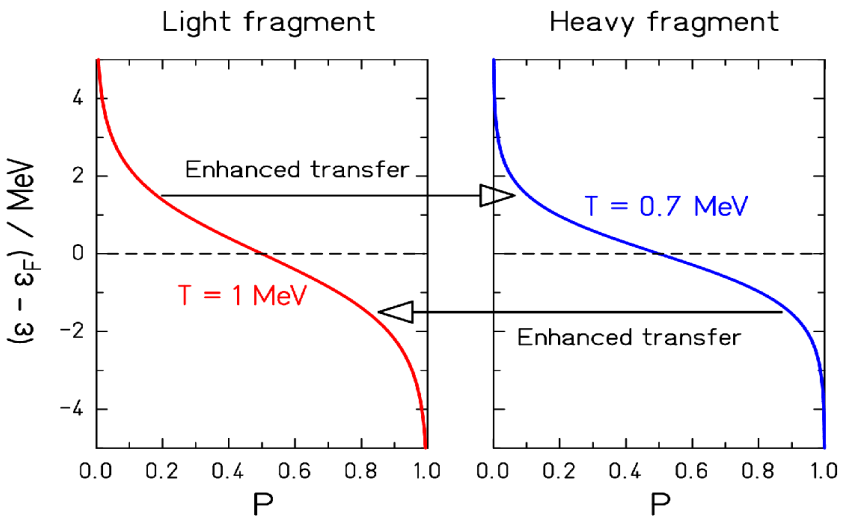

Figure 12. Single-particle occupation probabilities of the two nascent fragments in the pre-scission configuration.

According to this microscopic picture, the mean energy division is given by the condition that all nuclear states are populated with the same probability:

$$\bar{E}_1 = \frac{\int_0^E E_1 \rho_1(E_1) \rho_2(E-E_1) \mathrm{d}E_L}{\int_0^E \rho_1(E_1) \rho_2(E-E_1) \mathrm{d}E_L} \qquad (2)$$

The result is shown in figure 13 for a specific example. Obviously, the energy sorting is not complete: The light fragment keeps an excitation energy of about 2 MeV. This is a kind of border effect, because there are no levels below the nuclear ground state. However, there is a clear saturation of excitation energy in the light fragment, and any additional initial excitation energy is accumulated in the heavy fragment.

This energy sorting manifests itself in the mass-dependent neutron yields. Fig. 10 shows data for neutron-induced fission of ^{237}Np with E_n = 0.8 MeV and E_n = 5.55 MeV [63] as an example. The additional initial energy leads to an increased neutron yield from the heavy fragments, only. The behaviour is well reproduced by the GEF code, which includes a model for the process of energy sorting. The concentration of an increased initial excitation energy on the heavy fragment has also been found at somewhat higher excitation energies in proton-induced fission [71].

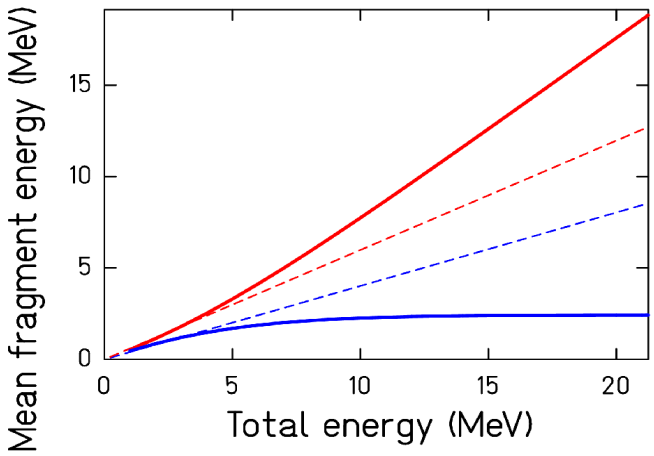

Figure 13. *Equilibrium mean energy division according to statistical equilibrium between the nascent fragments ^{94}Sr (blue full line) and ^{140}Xe (red full line) formed in ^{233}U(n,f). For comparison the energy division according to the mass ratio is shown (dashed lines).*

VI. EVEN-ODD EFFECT

Experimental systematics

The production of fragments with even Z is generally enhanced in low-energy fission. Figure 14 shows the Z distribution measured in electromagnetic-induced fission of ^{226}Th. In this nucleus, the symmetric fission channel is rather strong, see figure 4, and thus the even-odd effect could be measured over the whole fission-fragment range. This observation solved the long-standing question, whether there is an even-odd effect in the symmetric fission channel, since the yield at symmetry of systems accessible by thermal-neutron-induced fission is very low [72].

A systematic view on the local even-odd effect [73] in fission-fragment Z distributions [74] reveals a regular pattern and a general dependence on the fissioning system, see figure 15. The magnitude of the even-odd effect is small at symmetry, and it increases strongly with increasing asymmetry. At the same time, the even-odd effect generally decreases for heavier systems. The even-odd effect in the light fragment group of even-Z and odd-Z systems is essentially identical. When approaching symmetry, the even-odd effect in even-Z systems is described by the superfluid nuclear model [75], while it goes to exactly zero in odd-Z systems. Electromagnetic excitations lead to slightly higher excitation energies, thus reducing the magnitude of the even-odd effect. The large number of systems investigated [26] revealed that the appearance of a large even-odd effect at large asymmetry is a general phenomenon, also in odd-Z fissioning systems [76]. In any case, there is an enhancement for even-Z fragments in the light fragment group, indicating that it is the enhanced production of even-Z light fragments in their ground state, which is at the origin of the large even-odd effect at extreme asymmetry.

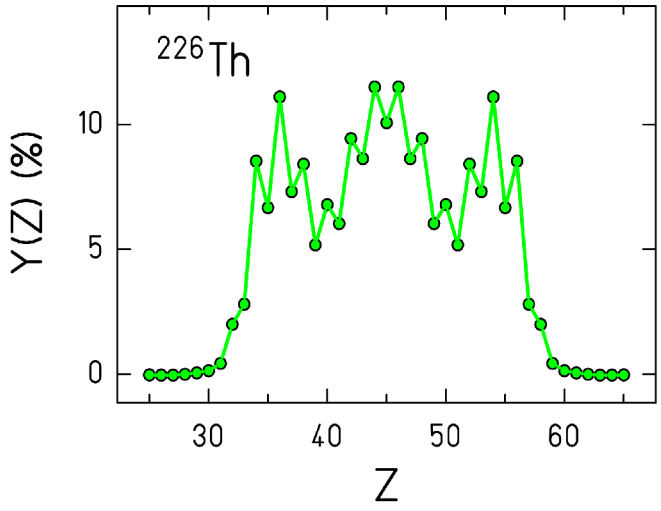

Figure 14: Fission-fragment element distribution measured in electromagnetic-induced fission of ^{226}Th [26].

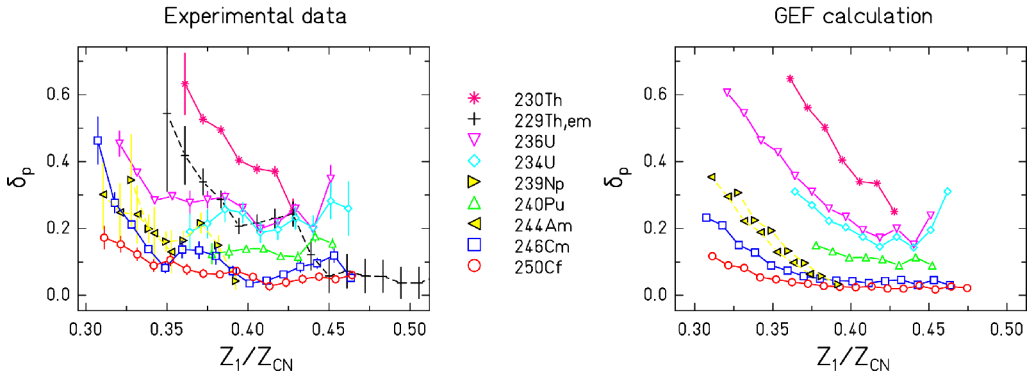

Figure 15. *Measured (left) and calculated (right) local even-odd effect in fission-fragment Z distributions in (n_{th},f) reactions. The fissioning nuclei are indicated. Data for fission of ^{229}Th, induced by electromagnetic excitations are included. See ref. [74] for references of the data.*

Final stage of energy sorting

It seems straightforward to attribute the enhanced production of even-*Z* light fragments to the energy-sorting mechanism [77] that explained already the differential behaviour of the prompt-neutron yields. If the time until scission is sufficient for the energy sorting to be accomplished, the system can still gain an additional amount of entropy by predominantly producing even-even light fragments. Compared to the production of odd-odd light fragments, the excitation energy of the heavy fragment increases by two times the pairing gap, and its entropy increases due to the increasing number of available states.

The right part of figure 15 shows a calculation with the GEF code, where this idea is included in a schematic way. The basic features are: (i) The excitation energy induced by dissipation grows with the Coulomb parameter $Z^2/A^{1/3}$, and the time needed for complete energy sorting is correspondingly increased. This explains the observed reduction of the even-odd effect for heavier systems. (ii) The thermal pressure grows with increasing asymmetry, which accelerates the energy-sorting process. This explains the strong increase of the even-odd effect at large asymmetry.

The asymmetry-driven even-odd effect is thus a threshold phenomena, which sets in when the time needed for reaching the scission configuration is sufficiently long for complete energy sorting. Fluctuations in the energy-sorting process are responsible for the smooth onset of the even-odd effect with increasing asymmetry.

VII. SUMMARY

New approaches extended the availability of fissioning systems for experimental studies on low-energy fission considerably and provided a full identification of all fission products in A and Z for the first time. The systematics of available data gives a more comprehensive view on the influence of shell effects and pairing correlations on the fission-fragment mass and nuclear-charge distributions. The previously claimed constant mean mass of the heavy component in asymmetric fission turned out to be biased by the restricted empirical knowledge. New data reveal that it is the position of the heavy component in Z, which is approximately constant. Theoretical arguments for this unexpected finding are not yet available.

The modelling of the fission process with dynamical models is still very difficult, since most advanced models in nuclear physics that have been developed for stationary states are not readily applicable to the decay of a meta-stable state. In addition, these models suffer from their tremendous demand on computing power, restricting severely the number of degrees of freedom to be investigated. Since quantum-mechanical effects are essential, stochastic approaches with classical models seem to be inadequate. Semi-empirical methods exploiting powerful theoretical ideas like (i) the separability of the influences of fragment shells and macroscopic influences of the compound nucleus, (ii) the properties of a quantum oscillator coupled to the heat bath of the other nuclear degrees of freedom for describing the fluctuations of normal collective modes, and (iii) an early freeze-out of collective motion to include dynamical effects seem to give a good description of the observed general trends.

The transformation of part of the fission Q value into intrinsic excitation energy along the fission process, following the laws of statistical mechanics, is essential for explaining the observed features of prompt-neutron emission and the even-odd effect in fission-fragment element yields. The threshold behaviour of the asymmetry-associated even-odd effect establishes a relation between the speed of the energy transfer between the nascent fragments and the dynamical time, starting at the moment when the two fragments develop their individual properties, e.g. their final temperatures, and the moment when the resistance against the transfer of protons across the neck becomes inhibitive. This new

insight stresses the importance of nuclear fission as a laboratory for studying the dynamics of non-equilibrium processes in mesoscopic objects under the influence of residual interactions.

Acknowledgements
This manuscript has been prepared in collaboration with Beatriz Jurado.

APPENDIX

The appendix repeats the comprehensive comparison of measured or evaluated fission-fragment mass and nuclear-charge distributions (figures 6, 7 and 8) with the results of the GEF code in linear scale. In this way, the quality of the reproduction of the highest mass yields can better be seen.

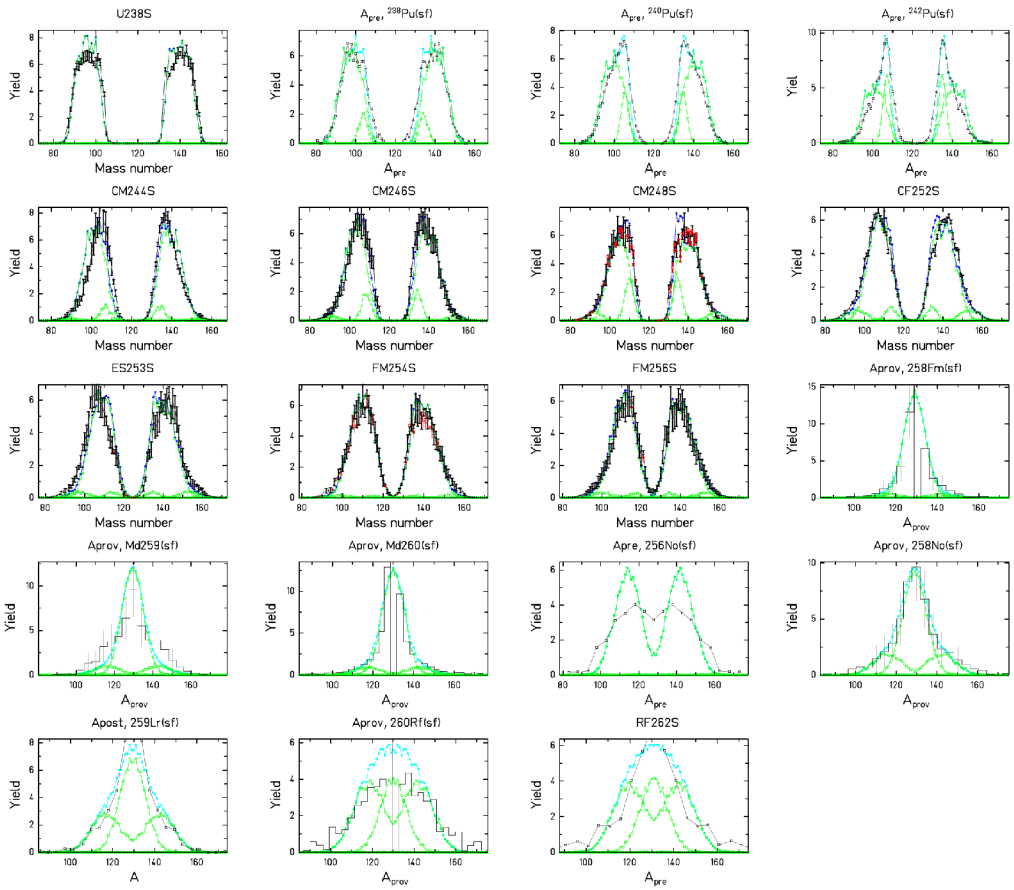

Figure A1*. Like figure 6, but in linear scale.*

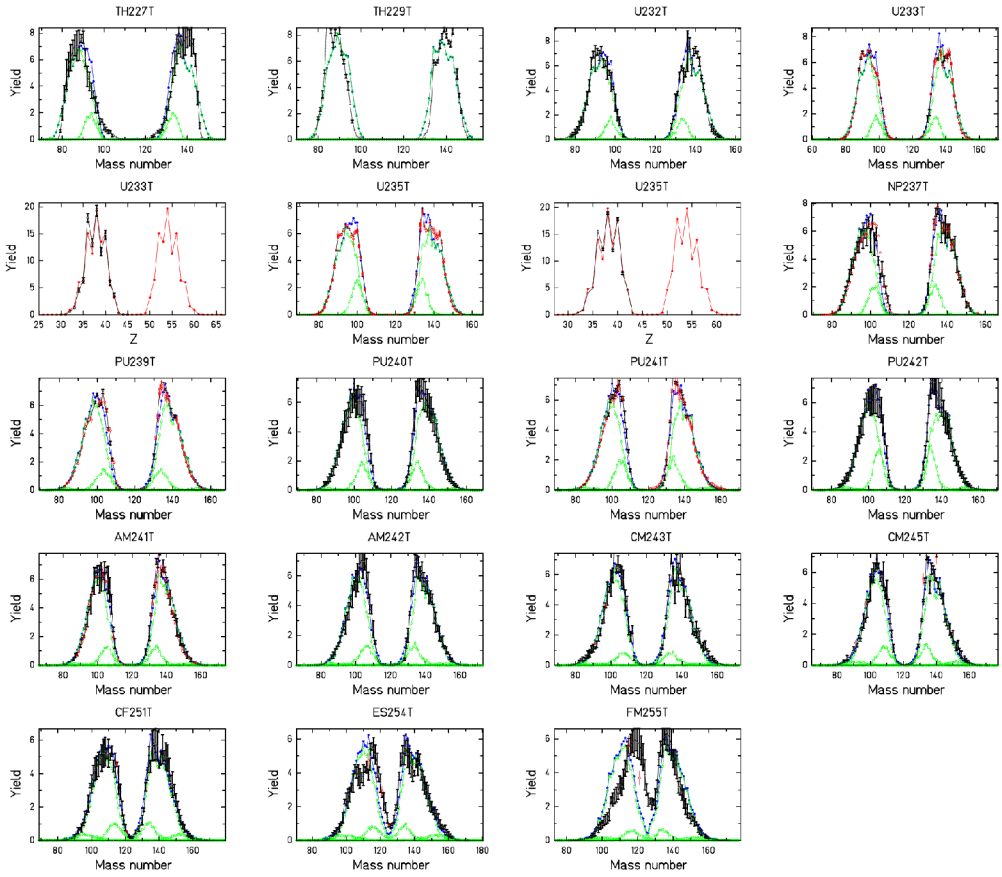

Figure A2. *Like figure 7, but in linear scale.*

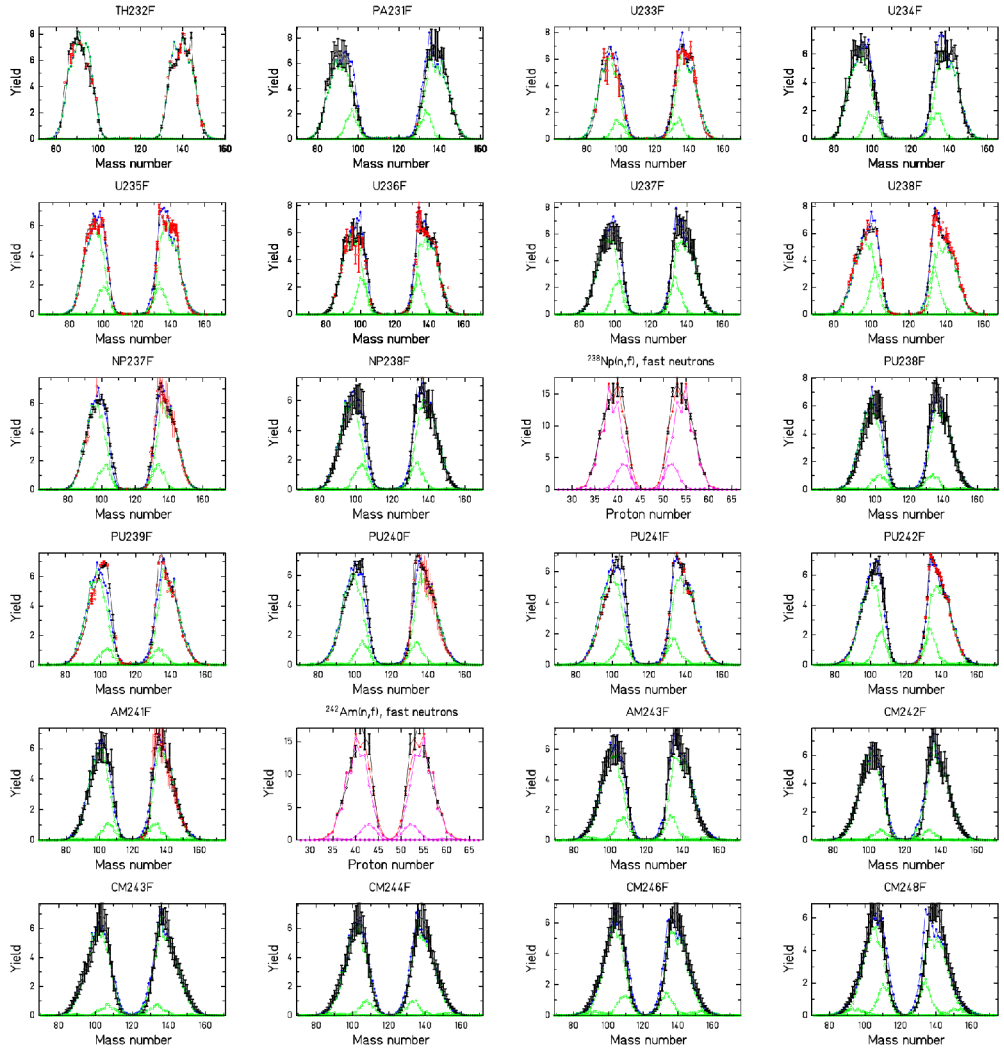

Figure A3. *Like figure 8, but in linear scale.*

1 Otto Hahn, Fritz Straßmann, Naturwissenschaften 27 (1939) 89.
2 N. Bohr, J. A. Wheeler, Phys. Rev. 56 (1939) 426.
3 M. Goeppert-Mayer, Phys. Rev. 74 (1948) 235.
4 O. Haxel, J. H. D. Jensen, H. E. Suess, Phys. Rev. 75 (1949) 1766.
5 S. G. Nilsson, Kgl. Danske Videnskab. Selskab, Mat.-Fys. Medd. 29 (1955) 16.
6 Nuclear Fission Process, C. Wagemans ed., CRC Press Inc., (1991).
7 U. Brosa, S. Grossmann, A. Müller, Phys. Rep. 197 (1990) 167.
8 H. Nifenecker et al., Z. Phys. A 308 (1982) 39.
9 J. P. Bocquet, R. Brissot, Nucl. Phys. A 502 (1989) 213c.
10 F.-K. Thielemann et al., Int. J. Mod. Phys. E 16 (2007) 114.
11 I. V. Panov et al., Nucl. Phys. A 747 (2005) 633.
12 J.-P. Delaroche et al., Nucl. Phys. A 771 (2006) 103.
13 D. Jacquet, M. Morjean, Prog. Part. Nucl. Phys. 63 (2009) 155.
14 K.-H. Schmidt, B. Jurado, Phys. Rev. C 82 (2011) 014607.
15 S. G. Kadmensky, Phys. Atom. Nuclei 70 (2007) 1628.
16 V. V. Pashkevich, Nucl. Phys. A 169 (1971) 275.
17 C. F. von Weizsäcker , Z. Phys. 96 (1935) 431.
18 H. Goutte et al., Intern. J. Mod. Phys. E 15 (2006) 292.
19 J. Randrup, P. Möller, Phys. Rev. Lett. 106 (2011) 132503.
20 C. Böckstiegel et al., Nucl. Phys. A 802 (2008) 12.
21 M. Caamaño et al., J. Phys. G: Nucl. Part. Phys. 38 (2011) 035101.
22 K.-H. Schmidt et al., Europh. Lett. 83 (2008) 32001.
23 http://www.cenbg.in2p3.fr/GEF, http://www.cenbg.in2p3.fr/GEFY
24 A. Ghiorso, T. Sikkeland, M. J. Nurmia, Phys. Rev. Lett. 18 (1967) 401.
25 A. N. Andreyev et al., Phys. Rev. Lett. 105 (2010) 252502.
26 K.-H. Schmidt et al., Nucl. Phys. A 665 (2000) 221.
27 F. Farget, private communication (2011).
28 A. N. Antonov et al. , Nucl. Instrum. Meth. A 637 (2011) 60.
29 E. A. C. Crough, At. Data and Nucl. Data Tables 19 (1977) 419.
30 W. E. Stein, Phys. Rev. 108 (1957) 94.
31 J. C. D. Milton and J. S. Fraser, Phys. Rev. 111 (1958) 877.
32 H. W. Schmitt, W. E. Kiker, C. W. Williams, Phys. Rev. 137 (1965) B837.
33 E. Moll et al., Nucl. Instrum. Methods 123 (1975) 615.
34 C. Donzaud et al., Eur. Phys. J. A 1 (1998) 407.
35 S. M. Polikanov , Sov. Phys. USPEKHI 15 (1973) 48
36 B. D. Wilkins, E. P. Steinberg, R. R. Chasman, Phys. Rev. C 14 (1976) 1832.
37 M. G. Itkis et al., Sov. J. Nucl. Phys. 52 (1990) 601.
38 S. I. Mulgin, K.-H. Schmidt, A. Grewe, S. V. Zhdanov, Nucl. Phys. A 640 (1998) 375.
39 J. P. Unik et al., Proc. Symp. Phys. Chem. Fission, Rochester 1973, IAEA Vienna (1974), vol. 2, p. 19.
40 I. Ragnarsson, R. K. Sheline, Phys. Scr. 29 (1984) 385.
41 M. Brack et al., Rev. Mod. Phys. 44 (1972) 320.
42 U. Mosel, H. Schmitt, Phys. Rev. C 4 (1971) 2185.
43 K.-H. Schmidt, A. Kelic, M. V. Ricciardi, Europh. Lett. 83 (2008) 32001.
44 A. S. Jensen, T. Døssing , Proc. Symp. Phys. Chem. Fission, Rochester 1973, IAEA Vienna (1974), vol. 1, p. 40.
45 D. Bucurescu, T. von Egidy, Phys. Rev. C 72 (2005) 06730.
46 A. V. Voinov et al., Phys. Rev. C 79 (2009) 031301.
47 A. V. Karpov, P. N. Nadtochy, D. V. Vanin, G. D. Adeev, Phys. Rev. C 63 (2001) 054610.

48 A. Ya. Rusanov, M. G. Itkis, V. N. Oklovich, Phys. At. Nucl. 60 (1997) 683.
49 A. V. Karpov, G. D. Adeev, Eur. Phys. J. A 14 (2002) 169.
50 H. Nifenecker, J. Physique Lett. 41 (1980) 47.
51 B. Bouzid et al., J. Phys. G: Nucl. Part. Phys. 24 (1998) 1029.
52 J. R. Nix, Ann. Phys. 41 (1967) 52.
53 L. Bonneau, P. Quentin, I. N. Mikhailov, Phys. Rev. C 75 (2007) 064313.
54 F. Gönnenwein, I. Tsekhanovich, V. Rubchenya, Intern. J. Mod. Phys. E 16 (2007) 410.
55 S. G. Kadmensky, Phys. Atom. Nuclei 71 (2008) 1193.
56 L. G. Moretto, G. F. Peaslee, G. J. Wozniak, Nucl. Phys. A 502 (1989) 453c.
57 H. Goutte, J. F. Berger, P. Casoli, D. Gogny, Phys. Rev. C 71 (2005) 024316.
58 J. Randrup, P. Möller, A. J. Sierk, Phys. Rev. C 84 (2011) 034613.
59 J. R. Nix, Nucl. Phys. A 130 (1969) 241.
60 V. M. Kolomietz, S. Åberg, S. V. Radionov, Phys. Rev. C 77 (2008) 014305.
61 W. J. Swiatecki, S. Bjørnholm, Phys. Rep. 4 (1972) 32.
62 N. Dubray, H. Goutte, J.-P. Delaroche, Phys. Rev. C 77 (2008) 014310.
63 A. A. Naqvi, F. Käppeler, F. Dickmann, R. Müller, Phys. Rev. C 34 (1986) 21.
64 E. Algin et al., Phys. Rev. C 78 (2008) 054321.
65 M. Guttormsen et al., Phys. Rev. C 68 (2003) 034311.
66 Y. Alhassid, G. F. Bertsch, L. Fang, Phys. Rev. C 68 (2003) 044322.
67 G. G. Dussel, S. Pittel, J. Dukelsky, P. Sarriguren, Phys. Rev. C 76 (2007) 011302.
68 K.-H. Schmidt, B. Jurado, Phys. Rev. Lett. 104 (2010) 21250.
69 K.-H. Schmidt, B. Jurado, Phys. Rev. C 83 (2011) 061601.
70 W. J. Swiatecki , Prog. Part. Nucl. Phys. 4 (1980) 383.
71 C. J. Bishop et al., Nucl. Phys. A 150 (1970) 12.
72 A. C. Wahl, Phys. Rev. C 32 (1985) 184.
73 B. L. Tracy et al., Phys. Rev. C 5 (1972) 222.
74 M. Caamaño, F. Rejmund, K.-H. Schmidt, J. Phys. G: Nucl. Part. Phys. 38 (2011) 035101.
75 F. Rejmund, A. V. Ignatyuk, A. R. Junghans, K.-H. Schmidt , Nucl. Phys. A 678 (2000) 215.
76 S. Steinhäuser et al., Nucl. Phys. A 634 (1998) 89.
77 K.-H. Schmidt. B. Jurado, arXiv:1007.0741v1[nucl-th] (2010).